THE PREDICTION OF MICROPITTING INITIATION ON GEAR TEETH: A NUMERICAL MODEL AND ITS CORRELATION WITH EXPERIMENTAL DATA

J. A. Brandão[1], J. O. Seabra[2], M. J. Castro[3]

[1]Bolseiro de investigação, INEGI, FEUP
[2]Prof. Associado, DEMEGI, FEUP
[3]Prof. Adjunto, Departamento de Engenharia Mecânica, ISEP

ABSTRACT

A numerical model for the prediction of micropitting initiation on gear teeth flanks and, to some extent, of mild wear is presented. This model hinges on a model of the mixed film lubrication regime and on the application of the Dang Van high-cycle multi-axial fatigue criterion. A comparison of an actual micropitting test on spur gears with its simulation using the model is made with regard to the mass loss of the driving gear and the evolution of its roughness.

1- INTRODUCTION

The trend in gear design has been, for the past few decades, in an improvement of the gear materials and surface treatments. This, alongside the improvement in lubricant oils formulation has allowed for ever higher speeds and power density in gear boxes. These improvements have helped in reducing the effect of the most destructive kinds of fatigue damage. In particular, the sort of progressive, in-depth originated fatigue damages, whose most characteristic example is the spalling damage, have been greatly reduced. As a result, surface originated fatigue damage have gained importance in the determination of the life of a gear [1] [2].

These types of damage, and preponderant among them the micropitting damage, come from the propagation of cracks that initiate at the surface of the gear and progress, first inward and then outward,

until a surface pit is produced [3]. A crucial characteristic of these fatigue cracks is that they have a very short propagation time [1]. Thus, in practice, the total life of a crack is equal to the initiation time. In this setting, an initiation model is very useful when dealing with such a fatigue mechanism.

Because these types of damage develop wholly within the first few tens of micrometers of the depth below the surface of a tooth, the important stress perturbations caused by the interaction of the roughness of the teeth cannot be ignored [4] [5]. In practise, this translates itself in the need for the solution of the lubrication problem in the mixed film regime, in which important surface pressure distributions occur due to the interaction of the roughness peaks of each tooth with the surface of the opposing one, be that interaction through direct metal-metal contact, be it mediated by a very thin, highly pressurized lubricating film [6].

This work concerns itself with the prediction of micropitting damage and mild wear in a spur gear. Micropitting is mainly defined by the small size of its pits, typically in the order of 10 μm in width and depth [7]. While not immediately destructive, the appearance of micropitting on the surface of a gear results in an increase in the noise level and in the geometric inaccuracy of the teeth, causing a loss in efficiency of the transmission. In extreme cases, a crack originating in a micropit may progress in depth with catastrophic consequences. Another possible scenario is that widespread micropitting so weakens the surface that a layer of material is removed at once [8].

The aim of this work is to provide a numerical model for the prediction of the initiation of micropitting fatigue cracks and mild wear. This model hinges on the solution of the contact problem between gear teeth, characterized by the mixed film regime of elastohydrodinamic lubrication, and on the application of the Dang Van high cycle multiaxial fatigue criterion, selected for its suitability for the prediction of fatigue crack initiation in complex loading cases.

2- OVERVIEW OF THE MODEL

A scheme of the model is shown in Figure 1. For a more complete exposition, the reader is referred to [9].

As shown in the figure, in a first phase, the model iterates through time to determine the elastic stresses on a gear tooth at each instant. The most distinctive component of this phase is the solution of the mixed film lubrication contact problem, to be described in a later section. With the surface loads, the model proceeds to calculate the elastic stresses in the gear tooth.
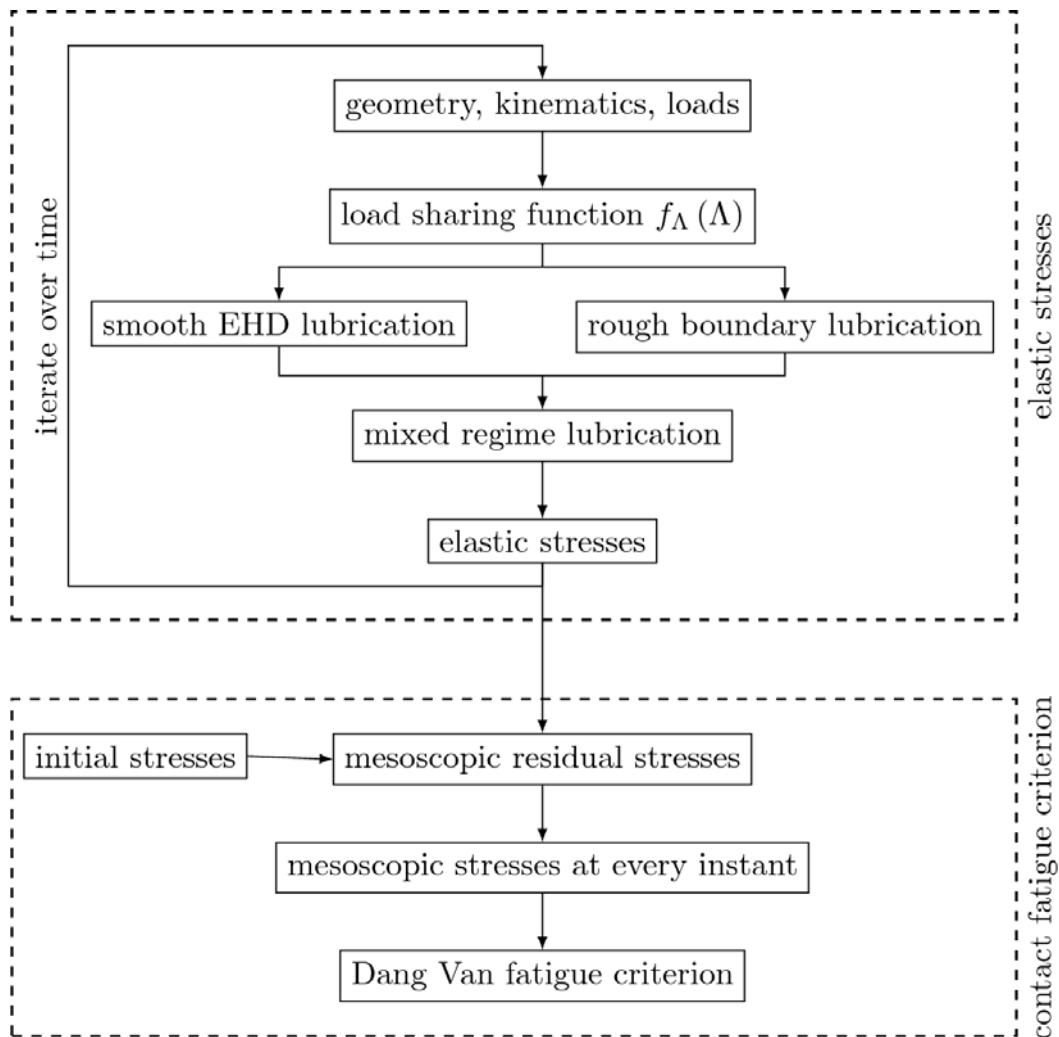

Fig 1: Scheme of the model operation.

Figure 2 shows a pressure distribution on the surface of a gear tooth flank with the corresponding octahedral shear stress field at an arbitrary instant in the meshing cycle.

The second phase of the model, which corresponds to the fatigue calculations, comes now into play. The Dang Van fatigue crack initiation criterion is applied to each material point within the first 20 μm of the depth of the tooth, in order to isolate the surface fatigue initiation from other fatigue phenomena.

3- MIXED FILM LUBRICATION

The contact between meshing gears is characterized by elasto-hydrodynamic (EHD) lubrication. EHD lubrication can be classified as full film EHD when the composite roughness of the contacting surfaces is negligible compared to the lubricant oil film thickness, as mixed film lubrication when the film thickness, while still carrying load, does not guarantee a complete separation of the gear flanks surfaces and as boundary film lubrication

when there is no longer a load carrying lubricating film. The relevant parameter in this classification is the specific film thickness (Λ) defined as:

$$\Lambda = \frac{h^{idealEHD}}{R_q^{composite}} \qquad (1)$$

where $h^{idealEHL}$ is the lubricant film thickness of the ideally smooth EHD case and $R_q^{composite}$ is the composite R_q roughness of the contacting surfaces.

Thus, and according to Vergne [10], the contacts are classified as:

- $\Lambda > 3$ full-film EHD lubrication,

- $3 > \Lambda > 2$ nearly full-film EHD with occasional contact between asperities,

- $2 > \Lambda > 1$ mixed lubrication in which the load is borne partly by direct naked contact between the surfaces and partly by a lubricating film,

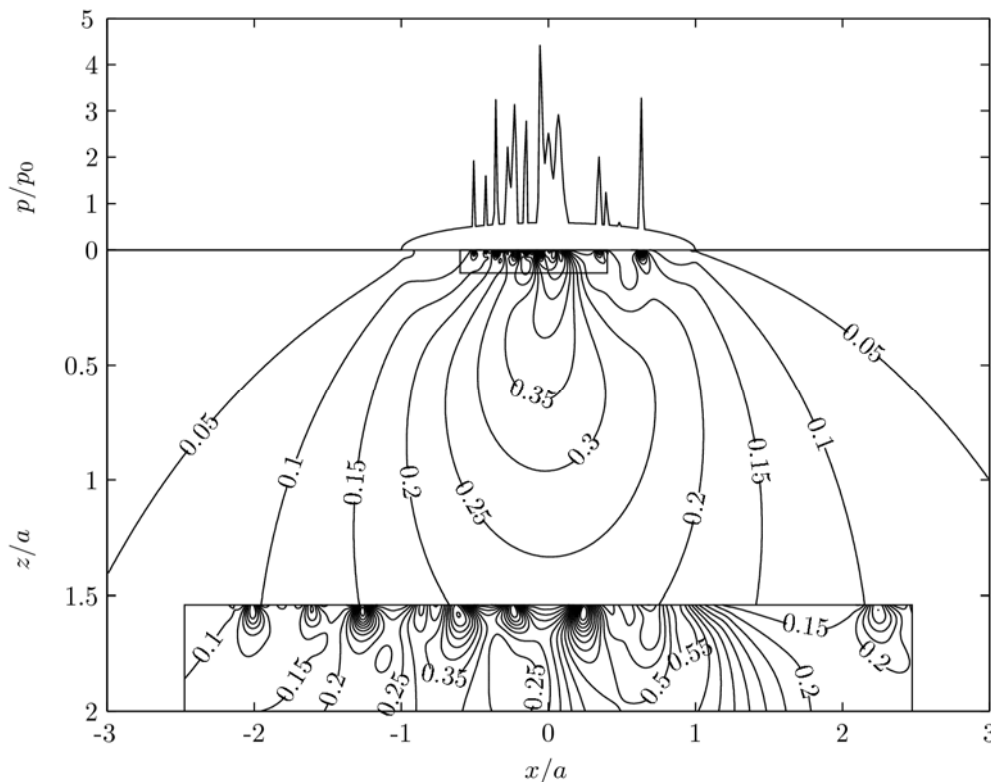- $1 > \Lambda$ boundary lubrication in which the load is borne almost exclusively by

Fig 2: Octahedral shear stress and pressure distribution of a gear tooth. The loads include a friction coefficient of 0.05.

- direct contact, although the friction coefficient is not so high as that found in the case of dry contact because of the presence of lubricant molecules that cling to the surfaces.

The model used here for mixed film lubrication is a modified version of that presented in [11] by Castro.

The contact load f_N may be divided into that borne by the lubricant f_N^{EHD} and that borne by direct contact between the surfaces f_N^{BDR}, so that:

$$f_N = f_N^{EHD} + f_N^{BDR} \qquad (2)$$

where:

$$f_N = \int_{-\infty}^{+\infty} p \ dx$$
$$f_N^{EHD} = \int_{-\infty}^{+\infty} p^{EHD} dx \qquad (3)$$
$$f_N^{BDR} = \int_{-\infty}^{+\infty} p^{BDR} dx$$

Let a load sharing function f_Λ be defined such that:

$$f_\Lambda = \frac{f_N^{EHD}}{f_N} \qquad (4)$$

and let is be supposed that, approximately:

- the load sharing function is, for each combination of lubricant oil and roughness orientation, only dependant on the specific film thickness Λ;

- the pressure distribution within the contact is the same as the overall load sharing distribution so that:

$$f_\Lambda = \frac{p^{EHD}(x)}{p(x)} \text{ for all} \qquad (5)$$

With the knowledge of this load sharing function it is possible to separate the very difficult problem of mixed film lubrication into two simpler ones: the perfectly smooth EHD and rough boundary lubrication problems.
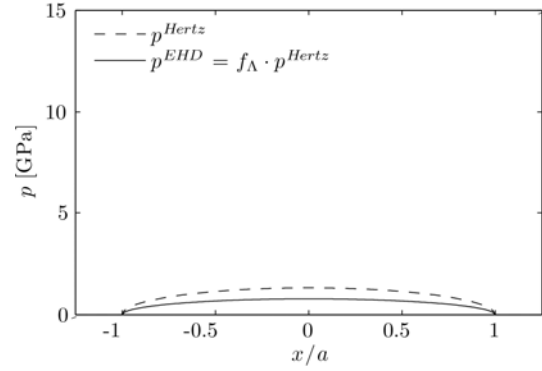

Fig 3: Distribution of the surface pressure borne by the lubricating film.

The surface pressures resultant from a perfectly smooth EHD lubrication can readily be approximated by the Hertzian pressure distribution, so that the pressure borne by the lubricating film becomes:

$$p^{EHD} = f_\Lambda \cdot p^{Hertz} \qquad (5)$$

This is illustrated in Figure 3.

Similarly, the pressure borne by direct contact between surfaces can be approximated by:

$$p^{BDR} = (1 - f_\Lambda) \cdot p^{BDR.T} \qquad (6)$$

where $p^{BDR.T}$ is the pressure distribution obtained when solving the problem of boundary film lubrication. This is illustrated in Figure 4.
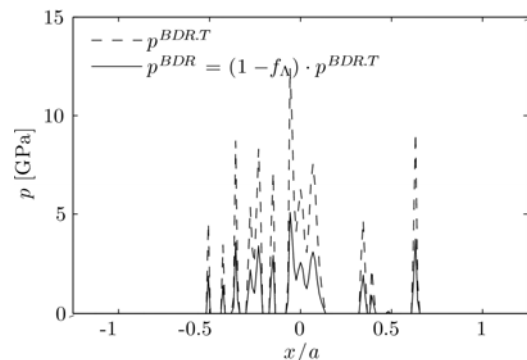

Fig 4: Distribution of the surface pressure borne by direct contact.

The total pressure distribution is simply obtained by summing these partial pressure distributions, as shown in Figure 5.
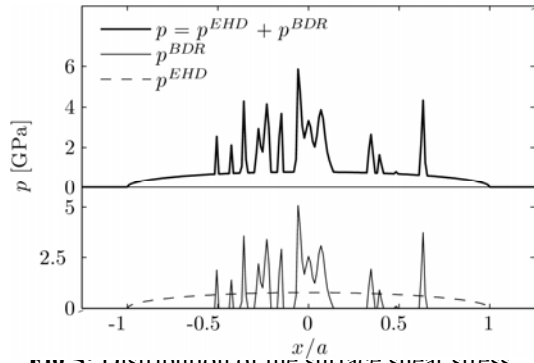
4

Fig 5: Distribution of the surface shear stress.

The problem of obtaining the surface shear stress τ (horizontal loads distribution) remains. These loads are obtained by summing the surface shear stress from the pressure distribution p^{EHD} with the surface shear from the pressure distribution p^{BDR}.

The surface shear from p^{EHD} is obtained by introducing that pressure distribution and the rheology of the lubricant oil into the Tevaarvek thermal equations [12].

The surface shear from p^{BDR} is obtained by considering that, in boundary film lubrication, the friction coefficient μ^{BDR} can be considered constant [13] so that:

$$\tau^{BDR} = \mu^{BDR} \cdot p^{BDR} \qquad (7)$$

As shown in Figure 6 the resulting surface shear stress is obtained by summing the partial shear stresses:

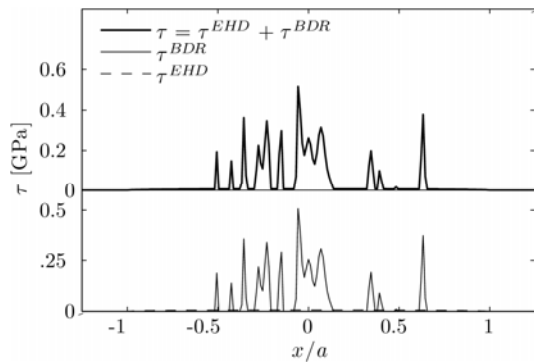$$\tau = \tau^{EHD} + \tau^{BDR} \qquad (8)$$

Fig 6: Distribution of the surface shear stress.

4- CONTACT FATIGUE CRITERION

Once the elastic stresses and the initial stresses (stresses due to the manufacturing processes such as cutting, heat treatment and grinding) the data needed to apply the Dang Van fatigue criterion are available. Dang Van [14] makes a distinction between the macroscopic stresses σ (in this case, the sum of the initial and elastic stresses already known at this point) and the mesoscopic stresses Σ, the stresses when considering the scale of a few grains. The first step in applying his fatigue criterion is the determination of the mesoscopic stresses from the macroscopic ones. This is effected by considering that each material point in the gear suffers elastic shakedown so that the mesoscopic stresses are the sum of the macroscopic stresses with mesoscopic residual stresses ρ (whose tensor is always deviatoric). In tensor notation, this yields:

$$\widetilde{\Sigma} = \widetilde{\sigma} + \widetilde{\rho} \qquad (9)$$

The mesoscopic residual stress tensor $\widetilde{\rho}$ is selected so that it solves the optimization problem:

$$
\begin{aligned}
g(\widetilde{\rho}) &= \max_t \left[-J_2\left(\sigma(t) + \widetilde{\rho}'\right) \right] \\
\widetilde{\rho} &: g(\widetilde{\rho}) = \min_{\widetilde{\rho}} g(\widetilde{\rho}')
\end{aligned} \qquad (10)
$$

where J_2 denotes the second invariant of the deviatoric tensor.

As was explained by Dang Van [14] and again by Desimone et al. [15], this is equivalent to the smallest enclosing ball problem of computational geometry. They

Table 1: Properties of the gear steel.

Property	Value
Young's modulus of elasticity	210 GPa
Poisson ratio	0.3
Density	7850 kg m^{-3}
Thermal conductivity	42 W m^{-1} K^{-1}
Specific heat capacity	0.46 kJ kg^{-1} K^{-1}

then proposed an algorithm to solve this problem. It has been found that a better procedure can be found in [16].

The Dang Van high-cycle multi-axial fatigue criterion is applied to the obtained mesoscopic stresses. It may be stated thus:

$$\tau_{max} + \alpha_{DV} \cdot p_H \leq \beta_{DV} \qquad (11)$$

where τ_{max} is the maximum mesoscopic shear stress, p_H is the hydrostatic stress (negative in compression) and α_{DV} and β_{DV} are fatigue properties of the gear material. In particular, β_{DV} can be interpreted as the fatigue limit of an alternate torsion test. In order that no fatigue crack initiation occurs at a given material point, Equation 12 must be respected at all instants of the load cycle.

An auxiliary quantity may be derived from Equation 12 thus:

$$\beta_{eq} = max_t \left(\tau_{max} + \alpha_{DV} \cdot p_H \right) \qquad (12)$$

This may be interpreted as the maximum shear stress in a reversed torsion test that is equivalent to the stress cycle undergone by the particular material point under analysis. Thus, the fatigue criterion may be reformulated as:

$$\beta_{eq} \leq \beta_{DV} \qquad (13)$$

5- SIMULATION OF A GEAR MICRO-PITTIN TEST

Cardoso [7] performed an actual gear micropitting test on FZG type C spur gears.

Table 2: Properties of the lubricant oil.

Parameter	Method	Desig.	Units	Lubricating Oils
Lubricant maker				**EXXON MOBIL**
Country				USA
Oil type		/	/	Industrial gear oil
Base oil	DIN 51451	/	/	Paraffinic mineral oil
Lubricant reference				**M1**(Mineral 1)
Physical properties				
Density @ 15ºC	DIN 51757	ρ_{15}	g/cm^3	0.894
Kinematic Viscosity @ 40 ºC	DIN 51562	ν_{40}	cSt	153.6
Kinematic Viscosity @ 100 ºC	DIN 51562	ν_{100}	cSt	14.4
Viscosity Index	DIN ISO 2909	*VI*	/	96
Pour point	DIN ISO 3106		ºC	-27
Wear properties				
KVA weld load	DIN 51350-2	/	N	2200
KVA wear scar (1h/300N)	DIN 51350-3	/	mm	0.32
Brugger	DIN 51347-2	/	N/mm^2	68
FZG rating	DIN 513540	K_{FZG}	/	>12

Table 3: Operating conditions of the gear micropitting test.

load stage	K3	K6	K8	K9
angular velocities	n_1 = 2250 RPM n_2 = 1500 RPM			
normal load F_N	851.34 N	2923.5 N	5072.6 N	6373.2 N
oil temperature	80 ºC	90 ºC		
duration	1 h	16 h		
number of cycles of the driving gear	135×10^3	2.16×10^6		

Table 4: Parameters used in the simulations.

μ^{BDR}	0.08	0.10	0.12	0.14
Load sharing function $f_\Lambda = \tanh\!\left(a_\Lambda \cdot \Lambda^{b_\Lambda}\right)$				
a_Λ	1.318	1.614	1.800	1.925
b_Λ	0.270	0.243	0.213	0.187
Roelands viscosity $\ln\dfrac{\eta}{\eta_0} = \ln\dfrac{\eta_0}{6.31\cdot10^{-5}\,Pa\cdot s}\cdot\left[\left(\dfrac{T-138K}{T_0-138K}\right)^{-S_0}\cdot\left(1+\dfrac{p}{196GPa}\right)^{Z}-1\right]$				
T_0	363 K			
η_0	1.56×10^{-2} Pa·s			
S_0	1.28			
Z	0.608			
Limiting shear stress $\ln\dfrac{\tau}{\tau_{L0}} = \alpha_{\tau L}\cdot p + \beta_{\tau L}\left(T^{-1}-T_0^{-1}\right)$				
τ_{L0}	25 MPa			
$1/\alpha_{\tau L}$	588 MPa			
$\beta_{\tau L}$	0 K			
Fatigue properties				
α_{DV}	0.987			
β_{DV}	400, 440, 480 … 880			

Table 5: Test procedure and corresponding simulation procedure.

Test procedure	step	Simulation procedure
Clean the gears in an ultrasonic bath and dry them.	1	
Weigh the gears.	2	
Measure the gear flanks roughness.	3	Introduce the roughness of the gears into the model.
Mount the gears on the test rig and perform load stage K3 during 1 h.	4	Run the simulation of load stage K3.
Without removing the gears from the test rig, take a lubricant oil sample.	5	
Submit the gears to load stage K6 during 16 h.	6	Run the simulation of load stage K6 with the initial roughness (this will be referred as K3+K6).
Dismount the gears, clean them in an ultrasonic bath and dry them. Photograph the gear flanks surfaces.	7	
Weigh the gears and calculate the mass-loss.	8	Predict the mass-loss of the driving gear.
Measure the gear flanks roughness.	9	Introduce the measured roughness into the model.
Mount the gears on the test rig and perform load stage K8 during 16 h.	10	Run the simulation of load stage K8.
Dismount the gears, clean them in an ultrasonic bath and dry them. Photograph the gear flanks surfaces.	11	
Weigh the gears and calculate the mass-loss.	12	Predict the mass-loss of the driving gear.
Measure the gear flanks roughness.	13	Introduce the measured roughness into the model.
Mount the gears on the test rig and perform load stage K9 during 16 h.	14	Run the simulation of load stage K8.
Dismount the gears, clean them in an ultrasonic bath and dry them. Photograph the gear flanks surfaces.	15	
Weigh the gears and calculate the mass-loss.	16	Predict the mass-loss of the driving gear.
Measure the gear flanks roughness.	17	

The detailed explanation of the conditions of the test is described in [7]. Relevant to the present article are the operating conditions listed in Table 3 and the properties of the lubricant oil and gear steel (carburized steel) listed in Table 1 and 2.

The test procedure—based on the FZG specification DMGK micropitting short test GFKT-C/8.3/90—as well as the simulation procedure are described in Table 5.

At the time of the simulation, the load sharing function f_A, the boundary friction coefficient μ^{BDR} and the fatigue properties α_{DV} and β_{DV} were not known. To surmount this difficulty a series of simulations with different combinations of these parameters were done. The parameters and their values are listed in Table 4. Each column represents a combination of parameters that was used in a simulation. Thus the rightmost column represents a series of simulation performed using the parameter values:

$$\mu^{BDR} = 0.14$$
$$f_A = \tanh\left(1.925 \cdot \Lambda^{0.187}\right)$$
$$\ln \frac{\eta}{1.56 \times 10^{-2} Pa \cdot s} = 5.51$$
$$\left[\left(\frac{T - 138K}{225K}\right)^{-S_0} \cdot \left(1 + \frac{p}{196 GPa^Z}\right) - 1\right] \quad (14)$$
$$\ln \frac{\tau_L}{25 MPa} = \frac{p}{588 MPa}$$
every value of
$$\beta_{DV} \in \{400, 440 \ldots 880\}$$

The non-linear rheology of the lubricant oil is obtained from the Bair and Winer visco-plastic equation [12]:

$$\dot{\gamma} = -\frac{\tau_L}{\eta} \ln\left(1 - \frac{\tau}{\tau_L}\right) \quad (15)$$

Figure 7 shows the graphs of the load sharing functions used with each boundary friction coefficient.

6- SOME SIMULATION RESULTS

Some interesting results of the simulation corresponding to the rightmost

column of Table 4 when β_{DV} has a value of 440 GPa are discussed here. It is interesting to note that the material points that violate the Dang Van criterion appear in patches. Focusing on a detail of the cross-section of the driving teeth, such a "patch" can be seen in Figure 8. Additionally, point Q is marked for further analysis.

In Figure 9, the successive positions of the cycle undergone by point Q in the plane p_H / τ_{max} are plotted. Some isolines of $\left(\tau_{max} + \alpha_{DV} \cdot p_H\right)$ are drawn as well. Note in particular the straight line where $\tau_{max} + \alpha_{DV} \cdot p_H = \beta_{DV}$ which corresponds to the limit of the Dang Van criterion. Since the cycle crosses this line, the material point violates the criterion, which was already known from Figure 8.

What is interesting is that the most unfavourable instant in the cycle is the rightmost tip in the graph. This means that the worst situation arises when the point is out of the contact.

This shows that one must distinguish between two types of residual stresses: the initial stresses, which always have a beneficial effect so long as they are compressive, since their deviatoric part is eliminated in the transition from macroscopic to mesoscopic stresses; and the mesoscopic residual stresses caused by the contact loads, which are always detrimental. Thus the residual stresses are the crucial factor in the formation of contact fatigue cracks and the transient stress states that occur when a point travels through the contact are much less important.
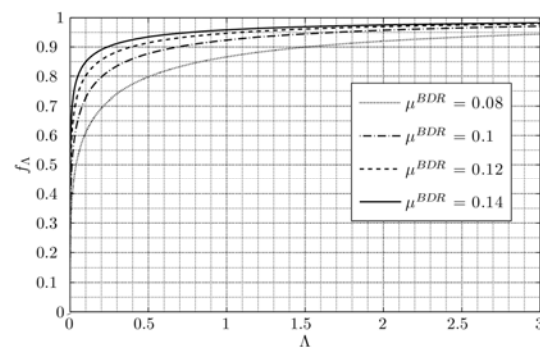

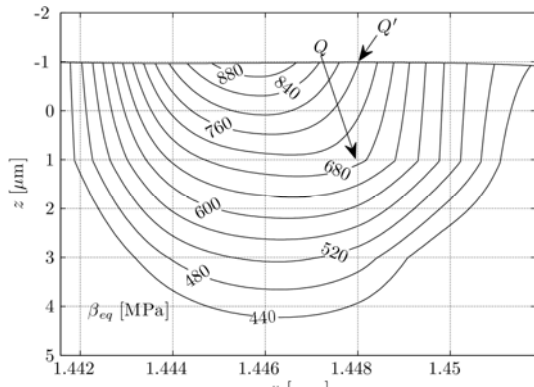**Fig 7**: The load sharing functions used in the simulations.

Fig 8: A patch of material points where fatigue crack initiation is predicted by the model: $\beta_{eq} > \beta_{DV}$.
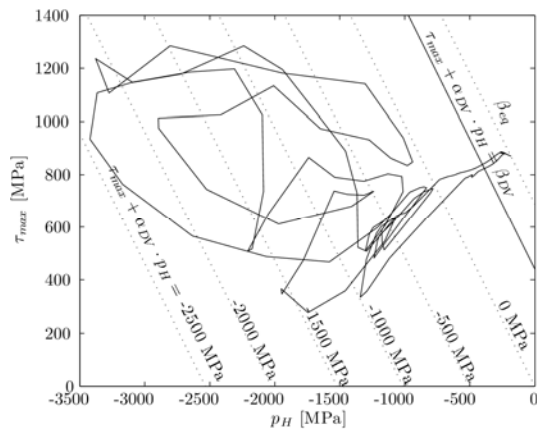

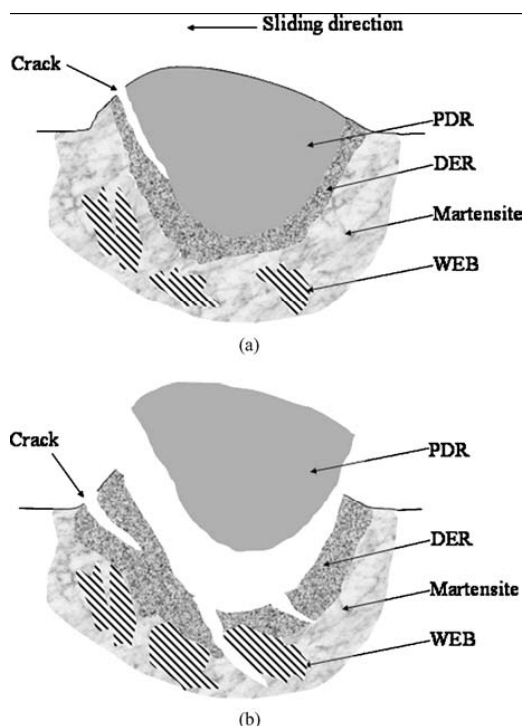**Fig 9**: Plot of the cycle undergone by a material point in the p_H / τ_{max} plane.

Fig 10: Schemtic representation of the formation of a micropit according to Oila and Bull [3].

7- COMPARISON OF THE SIMULATIONS WITH THE TEST

Taking another look at Figure 8, it is obvious that not all material points within the patch will be at the origin of a fatigue crack. The first crack to develop should pre-empt the formation of another. It is impossible to decide which will be the "winner" within the framework of the Dang Van fatigue criterion. Thus, there is no obvious way to compare the results of a test, which deals with the "completed" micropits, with the simulations, which indicate sites of *initiation*.

It is interesting to compare the patch in Figure 8 with the schematic representation of the formation of a micropit in Figure 10, which was taken from the article [3] by Oila and Bull. The similarity in shape and size (though this is not shown in Figure 10) are striking.

On the strength of this similarity, an approximate prediction of mass-loss in the driving gear through contact fatigue is proposed defined by:

$$m_{DV} = Z_1 \cdot A_{DV} \cdot b \cdot \rho_{steel} \qquad (16)$$

where m_{DV} is the predicted mass-loss, Z_1 is the number of teeth in the driving gear, A_{DV} is the total area of the patches of violation of the Dang Van criterion on the flank of one tooth, b is the face width of the gear and ρ_{steel} is the volumetric mass of the gear steel.

There is a qualitative argument in favour of this. The region marked as PDR in Figure 10 was described in [3] as a region where heavy plastic deformation occurs, to the point that the steel is in a different crystallographic phase. On the other hand, it was seen that the patches of violation such as the one in Figure 8 are in direct relation with the residual stresses in the tooth flank. It is therefore to be expected that a rough equivalence should exist between the PDR and the patches of violation of the Dang Van criterion.

In Table 6, the values of the predicted mass-loss of the driving gear in each stage

are compared to the measured ones. The predicted mass-loss values are shown only for two distinct simulation cases. As an additional information, the predicted mass-loss above and bellow the pitch line are also listed, as well as the specific mass-loss: the mass-loss per length of tooth.

The absolute mass-loss of the gear is also shown in Figure 11 in a somewhat more readable form.

In both Table 6 and Figure 11, the designation K3+K6 corresponds to the combined mass-loss of load stages K3 (a running-in stage) and K6. These load stages are so bundled because no mass-loss measurement was made at the end of load stage K3 of the micropitting test.

The first striking fact to emerge from the data is that the simulation of stage K3+K6 (initial roughness combined with the operating conditions of load stage K6) is utterly wrong. There is a simple reason for this: in the simulations, the relatively high loads of the K6 stage were applied to the initial roughnesses. It is therefore unreasonable to expect good results. On might also impute the bad results to a deficiency of the model, but the results of the simulations of load stage K3 alone give plausible results, although there is no actual measurements against which to compare them.

Another striking fact, is that the simulation case 1 results are in remarkable agreement with the measurements of load stages K8 and K9. Indeed, even the simulations case 2 gives results that are very nearly parallel to the measurements in Figure 11. The same is true of every others simulations that were run, although their results are not shown here for the sake of clarity. This seems to indicate a strong correlation between the total area of patches of violation of the Dang Van criterion and the mass-loss in micropitting tests.

Turning one's attention to the part of Table 6 that details the results of simulation case 1, it is interesting to note that, at the end of load stage K8, the predicted specific mass-loss above the pitch line is much
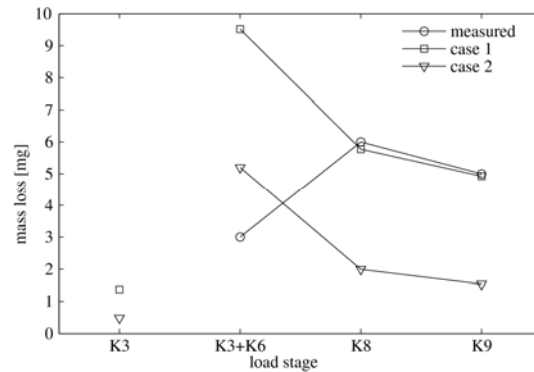

Fig 11: Mass loss of the driving gear in each stage.

lower than below it. In fact, it was reported in [7] by Cardoso that the micropits made their appearance precisely at the end of that load stage and exclusively below the pitch line. This is in agreement with the generally observed fact that the part of the flank of a driving gear that is below the pitch line is more prone to micropitting.

8 CONCLUSIONS

A model was proposed for the initiation of micropitting cracks. It includes a model of mixed film lubrication and a model of fatigue initiation. A comparison was made of the measured mass-loss in a micropitting test with the predicted mass-loss of its simulation. The predicted values were shown to be in good agreement with the measured ones.

A final note needs to be made as to the good results of the mass-loss prediction. There must have been some mass lost due to wear of the surfaces during the tests. Therefore, this seems to indicate that the model not only deals with micropitting, but also with mild wear, inasmuch as it is caused by contact fatigue.

While these results are far from conclusive, they warrant some further work on the model. Notably a more extensive round of tests should be performed to decide of the validity of the model.

Table 6: Comparison of the measured mass loss at the end of each load stage with the predicted one. The predicted mass loss values are separated into mass loss below the pitch line and above it. Also listed are the specific values of mass loss (mass loss per length of tooth).

Position	K3		K3+K6		K8		K9	
	absolute [mg]	specific [mg/mm]	absolute [mg]	specific [mg/mm]	absolute [mg]	specific [mg/mm]	absolute [mg]	specific [mg/mm]
Model prediction, simulation case 1 μ_{BDR}=0.14 and β_{DV}=440 MPa.								
below pitch line	0.624	0.2387	3.946	1.511	2.463	0.9429	1.520	0.5821
above pitch line	0.750	0.1381	5.571	1.026	3.309	0.609	3.403	0.6265
whole tooth	1.374	0.1707	9.517	1.183	5.771	0.7174	4.924	0.612
Model prediction, simulation case 2 μ_{BDR}=0.12 and β_{DV}=560 MPa.								
below pitch line	0.227	0.0868	2.171	0.8312	0.9359	0.3583	0.3976	0.1522
above pitch line	0.255	0.0469	3.024	0.5567	1.057	0.1946	1.137	0.2094
whole tooth	0.482	0.0599	5.195	0.6458	1.993	0.2477	1.535	0.1908
Test measurements								
whole tooth	N/A	N/A	3	0.373	6	0.746	5	0.6214

REFERENCES

[1] G. Peridas, A. M. Korsunsky, D. A. Hills, The relationship between the Dang Van criterion and the traditional bulk fatigue criteria, The Journal of Strain Analysis for Engineering Design 38 (3) (2003) 201–206.

[2] F. Antoine, J.-M. Besson, Simplified modellization of gear micropitting, Journal of Aerospace Engineering 216 (6) (2002) 291–302.

[3] A. Oila, S. J. Bull, Phase transformations associated with micropitting in rolling/sliding contacts, Journal of Materials Science 40 (18).

[4] A. Oila, S. J. Bull, Assessment of the factors influencing micropitting in rolling/sliding contacts, Wear 258.

[5] T. Krantz, The influence of roughness on gear surface fatigue, NASA TM-2005-213958, ARL-TR-3134.

[6] J. Tao, T. G. Hughes, H. P. Evans, R. W. Snidle, N. A. Hopkinson, M. Talks, J. M. Starbuck, Elastohydrodynamic lubrication analysis of gear tooth surfaces from micropitting tests, Journal of Tribology 125 (2) (2003) 267–274.

[7] N. Cardoso, Mechanical performance of biodegradable, low toxicity ester based industrial oils, Master's thesis, Faculdade de Engenharia da Universidade do Porto (2007).

[8] L. Faure, Aspect des dentures d'engrenage après fonctionnement, Centre Technique des Industries Mécaniques, 1990.

[9] J. Brandão, Gear micropitting prediction using the Dang Van high-cycle fatigue criterion, Master's thesis, Faculdade de Engenharia da Universidade do Porto (2007).

[10] P. Vergne, Super low traction under EHD and mixed lubrication regimes, in: A. Erdemir, J.-M. Martin (Eds.), Superlubricity, Elsevier BV, 2007, pp. 429–445.

[11] J. Castro, Gripagem de engrenagens FZG lubrificadas com óleos base. Novos critérios de gripagem globais e locais, Ph.D. thesis, Faculdade de Engenharia da Universidade do Porto (2004).

[12] J. O. Seabra, A. Campos, A. Sottomayor, Lubrificação elastohidrodinámica, Faculdade de Engenharia da Universidade do Porto, 2002.

[13] R. C. Castle, C. H. Bovington, The behaviour of friction modifiers under boundary and mixed EHD conditions, Lubrication Science 15 (3) (2003) 253–263.

[14] K. Dang Van, B. Griveau, O. Message, On a new multiaxial fatigue limit criterion: theory and application, in: M. Brown, K. Miller (Eds.), Biaxial and Multiaxial Fatigue, EGF 3, Mechanical Engineering Publications, London, 1989, pp. 479–498.

[15] H. Desimone, A. Bernasconi, S. Beretta, On the application of the Dang Van criterion to rolling contact fatigue, Wear 262 (4-5) (2006) 567–572.

[16] B. Gärtner, Fast and robust smallest enclosing balls, in: Proc. 7th annu. European Symposium on Algorithms (ESA), Vol. 1643 of Lecture Notes in Computer Science, Springer-Verlag, 1999, pp. 325–338